JMEPEG (2019) 28:4826–4837
https://doi.org/10.1007/s11665-019-04260-3

1059-9495/$19.00

Effect of Friction Stir Processing on the Microhardness, Wear and Corrosion Behavior of Al6061 and Al6061/SiO_2 Nanocomposites

Yousef Mazaheri, Akbar Heidarpour, Mohammad Mahdi Jalilvand, and Masoud Roknian

(Submitted October 10, 2018; in revised form July 3, 2019; published online August 12, 2019)

An effect of the friction stir processing (FSP), its pass numbers and addition of the SiO_2 nanoparticles on microhardness, wear behavior and corrosion performance of the Al6061 aluminum alloy was investigated. Scanning electron microscopy (SEM) and optical microscopy were utilized to characterize the microstructure of the alloy, FSPed and composite samples. SEM observations revealed that the SiO_2 particles were not uniformly dispersed in the matrix after two passes of FSP. However, increasing the pass number more than two passes resulted in a great improvement in the distribution of the SiO_2 particles. The application of FSP led to overall softening compared to the base metal. Softening of the Al6061 alloy was probably attributed to the coarsening of Mg_2Si. Corrosion resistance of the FSPed samples found a significant reduction compared to the base metal. Applying higher pass number of the process and also addition of the SiO_2 nanoparticles improved the wear behavior of the samples.

Keywords Al6061, corrosion performance, friction stir processing, pass number, SiO_2 nanoparticles, wear behavior

1. Introduction

Because of the unique properties such as high strength-to-weight ratio, high ductility and high corrosion resistance, aluminum and its alloys have attracted great application in different industries, especially in aerospace and automotive (Ref 1, 2). However, poor wear resistance can be introduced as the major problem which limited their applications (Ref 3). Adding reinforcements into the aluminum alloys matrix can enhance their wear behavior (Ref 4). Fabrication of aluminum matrix composites (AMCs) is typically performed via casting and powder metallurgy methods (Ref 5). In spite of the different advantages of these methods, there could be several problems such as porosity in the matrix, debonding and poor wettability between the matrix and reinforcements (Ref 6-8).

Generally, in the case of bulk composites, a considerable loss in ductility and toughness restricted their broad applications. On the other hand, wear properties of the materials are influenced by their surface conditions. Accordingly, improving the surface properties of materials can be introduced as a useful way for enhancing their wear properties. In this situation, not only the component has a desirable toughness but also the reinforced surface provides a longer life (Ref 9). Therefore, surface modification by using reinforcements is adequate to improve the tribological properties of aluminum (Ref 10, 11). Friction stir processing (FSP) is an effective method for the fabrication of the surface composites (Ref 12-17). In this method, the reinforcing materials are squeezed into the grooves which are machined on the surface of the bulk material. Throughout FSP, rotation of the tool and friction between tool and work piece lead to high plastic deformation and heat increase which result in the grain refinement of the microstructure. Generally, three distinct zones including the stir zone (SZ), thermomechanically affected zone (TMAZ) and heat-affected zone (HAZ) can be identified through this process (Ref 18).

The particulate-reinforced AMCs have several advantages such as ease of fabrication, lower costs and isotropic properties related to the other types of composites (Ref 19). A growing body of literature has investigated the effect of FSP on mechanical and tribological properties of the aluminum alloys, as Al6061. In these studies, it is mentioned that the wear behavior of the Al6061 alloy can be enhanced by the incorporation of different reinforcing materials such as SiC (Ref 3, 20-23), SiO_2 (Ref 24), Al_2O_3 (Ref 3, 25), carbon nanotube (CNT) (Ref 26, 27), graphite (Ref 20, 28), NiTi (Ref 29) and TiB_2 (Ref 30, 31). In addition, some papers dealt with grain refinement by using FSP to enhance surface properties (Ref 32, 33). Also, some researchers fabricated hybrid surface composites and could obtain better results (Ref 3, 20, 25). For instance, Jalilvand et al. (Ref 34) fabricated A356-SiO_2-Al_2O_3 surface composites via FSP and showed enhanced mechanical and corrosion properties compared with A356 Al alloy and the FSPed A356. But the effects of FSP pass numbers were not studied in their investigation.

Hussain et al. (Ref 24) developed a SiO_2-reinforced AA6061 surface composite. The amorphous SiO_2 was produced by rice husk ash. They only investigated the microstructural evolution and hardness of the FSPed samples and found that microhardness of FSPed samples, either with SiO_2 particles or without them, was lower than that of the base metal. To the best knowledge of authors, the effect of FSP pass numbers on the mechanical, tribological and electrochemical behavior of

Yousef Mazaheri, Mohammad Mahdi Jalilvand, and **Masoud Roknian**, Department of Materials Engineering, Bu-Ali Sina University, Hamedan 65178-38695, Iran; and **Akbar Heidarpour**, Department of Metallurgy and Materials Engineering, Hamedan University of Technology, Hamedan 65155-579, Iran. Contact e-mail: y.mazaheri@basu.ac.ir.

Al6061 alloy and its surface composites has not been dealt with in depth and needs to be considered in future researches. Therefore, the objective of this study is to evaluate the microhardness, wear and corrosion behavior of Al6061/SiO_2 surface nanocomposite produced by FSP. Also, the effect of pass numbers on the dispersion and distribution of SiO_2 nanoparticles as well as the above-mentioned properties was studied.

2. Experimental Procedure

2.1 Materials and Fabrication of the Nanocomposites

In this study, to fabricate the surface composites, firstly Al6061 sheets with 150 × 50 × 6 mm^3 size were cut as the base materials. After that, SiO_2 nanoparticles (with the average particle size of 100 nm) were prepared as reinforcing materials. The SEM image with x-ray diffraction pattern (XRD) of the SiO_2 nanoparticles is shown in Fig. 1.

A FSP machine was equipped with a fixture in order to apply the process on the samples. The fixtures were designed in a way to keep specimens firm on the machine and prevent sample movement when the process was carrying out. In order to insert SiO_2 nanoparticles in the matrix, a groove of 2 mm × 2 mm was created on the base metal, and then SiO_2 powder was filled into the groove. To perform FSP, at first and after filling the groove with SiO_2 particles, a pin-less tool was used to close the groove. This guarantees powder packing and avoids powder spreading. Then, FSP was conducted by a tool with a square pin. The tool is made of H13 hot working steel. The diameter of shoulder was 20 mm. Also, the dimension of the square pin was 6 × 6 mm^2 and a length of 3 mm. In order to obtain sound specimen without flawless and to have the most properties, several combinations of speeds, both rotational and transverse, were tested. According to the results, the optimum sample was obtained for the tool rotational and transverse speeds of 500 rpm and 15 mm/min, respectively. Then, these speeds were chosen to process all samples. In addition, the rotation direction of the FSP tool was in the clockwise direction with a tilt angle of 3°.

2.2 Testing and Characterization

The optical microstructure of the FSPed samples was collected by an optical microscope of union equipped with a digital optical scanner. The composition of etchants used in this study consisted of 2 ml of HF, 3 ml of HCl, 20 ml of HNO_3 and 175 ml of distilled water (Keller's regent) and perchloric acid electrolyte. The microstructural characterizations of the friction stirred samples were analyzed by using a scanning electron microscope (Jeol, JSM 840) equipped with energy-dispersive spectroscopy (EDS).

The phase identification of the samples was done by x-ray diffraction (XRD, Asenware AW-DX300) with Cu target, Kα radiation (wavelength of 1.5406 Å), scanning step of 0.01 degree and time per step of 1 s.

According to the ASTM E384 standard (Ref 35), the hardness testing was conducted via micro-Vickers methods on the surface of the samples. Buehler's equipment (load of 100 g for 15 s) was employed for these tests.

Moreover, the tribological properties of the samples were studied utilizing a pin and disk tribometer at ambient temperature according to the ASTM G99 standard (Ref 36). In order to perform the wear tests, the pins were machined from samples and AISI D3 steel with the hardness value of 59 HRC was chosen as disk. The wear tests were conducted under the condition of sliding speed of 0.1 mm/s, the normal force of 20 N and sliding distance of 1000 m. The friction and wear test results were obtained from the at least mean of four readings.

The electrochemical behavior of the samples was studied using potentiodynamic set (Iviumstat compact 20250 H). Anodic–cathodic polarization curves were measured by immersion in 3.5 wt.% aqueous sodium chloride (NaCl) solution. Potentiodynamic tests were performed in a typical three-electrode cell with the sample as the working electrode, the platinum as the counter electrode and the saturated AgCl/Ag as the reference electrode. Prior to potentiodynamic tests, specimens were kept in the solution for 1 h in order to institute the

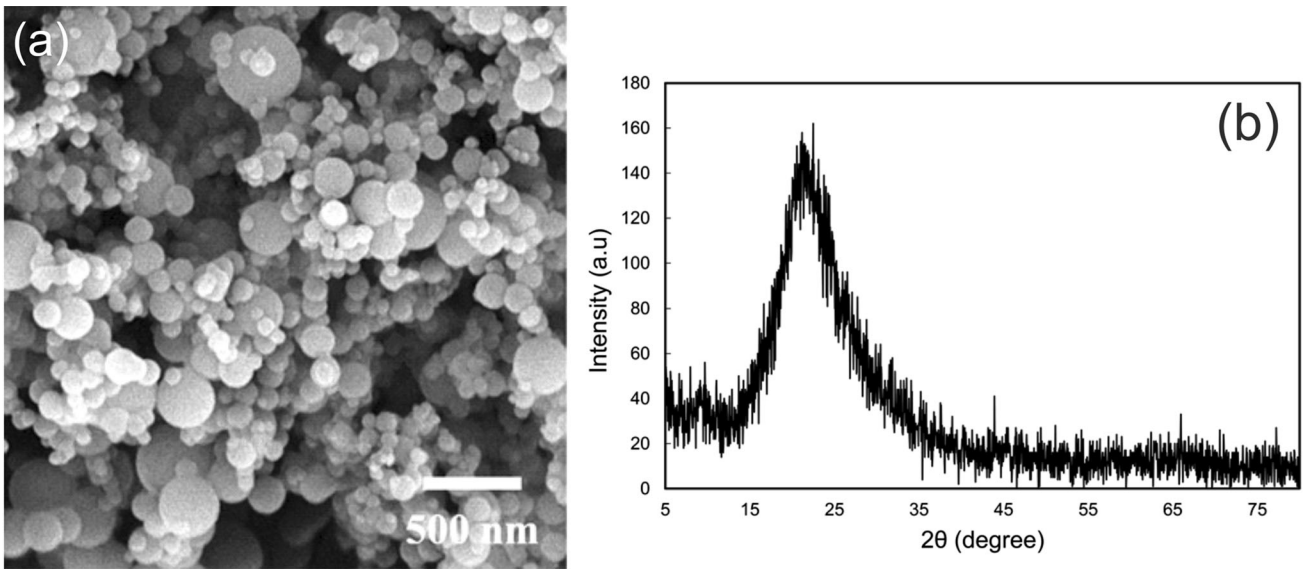

Fig. 1 (a) SEM micrograph and (b) XRD patterns of SiO_2 particles used as reinforcement

free corrosion potential (E_{corr}). Polarization curves were acquired at a scanning rate of 0.01 V/s from − 1.2 to 0.3 V.

3. Results and Discussion

3.1 Microstructures

The cross-sectional optical micrographs of two-pass FSPed Al6061 are shown in Fig. 2. The different microstructural regions including stir zone (SZ), thermomechanically affected zone (TMAZ) and base metal (BM) are shown in Fig. 2. In fact, the high thermal conductivity of the aluminum is the main reason for the disappearance of heat-affected zone (HAZ) in this figure. A comparison between the microstructures of the base metal and SZ region shown in Fig. 2 reveals that a grain size refining has occurred for the FSPed sample. In addition, Fig. 3 shows the cross-sectional optical micrograph of as-received Al6061 and SZ zone of samples with different pass numbers of the FSP. It is obvious that the FSP has led to the proper grain refinement of Al6061 for all samples.

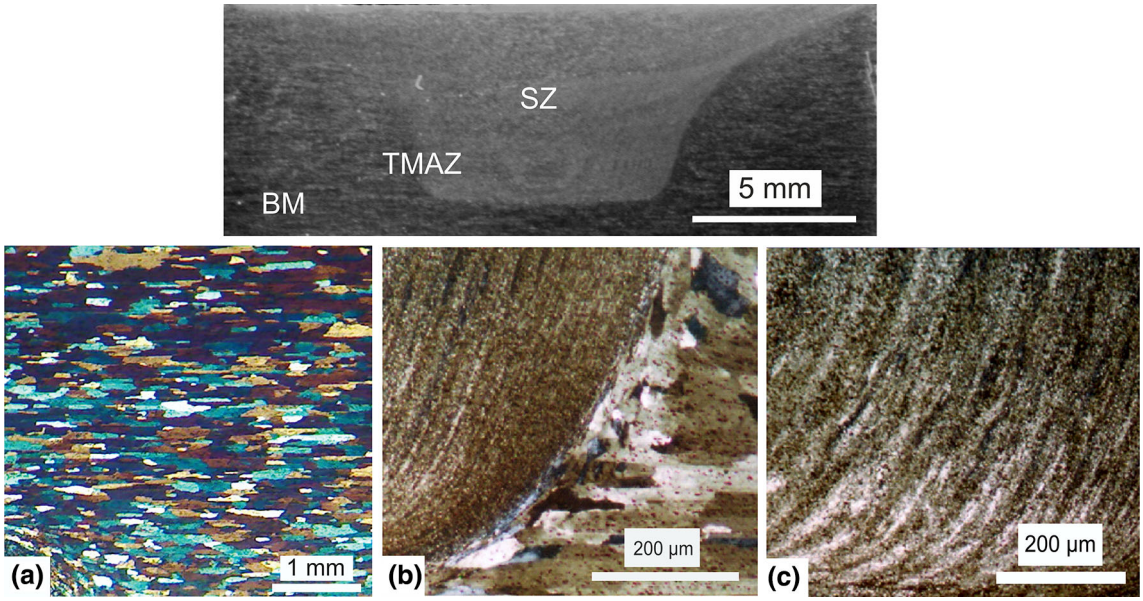

Fig. 2 Optical micrographs of two-pass FSPed Al6061 with different microstructural regions (a) base metal (BM), (b) thermomechanically affected zone (TMAZ) and (c) stir zone (SZ)

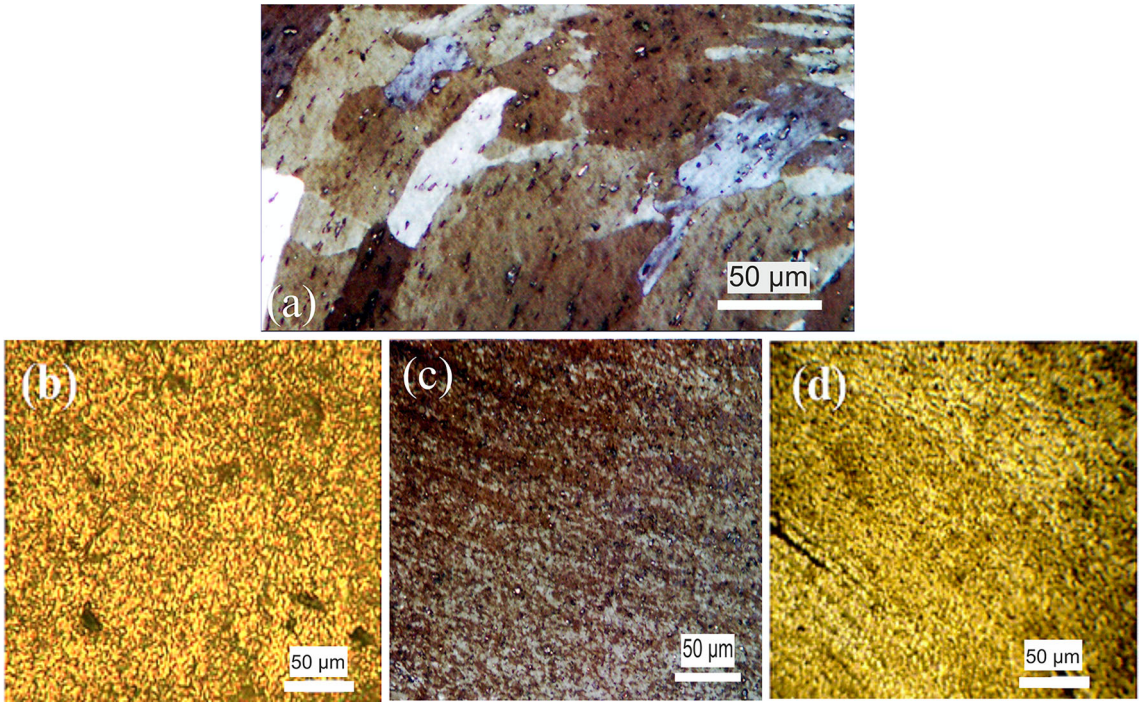

Fig. 3 The optical micrographs of (a) BM, (b) two-pass, (c) three-pass and (d) five-pass FSPed Al6061

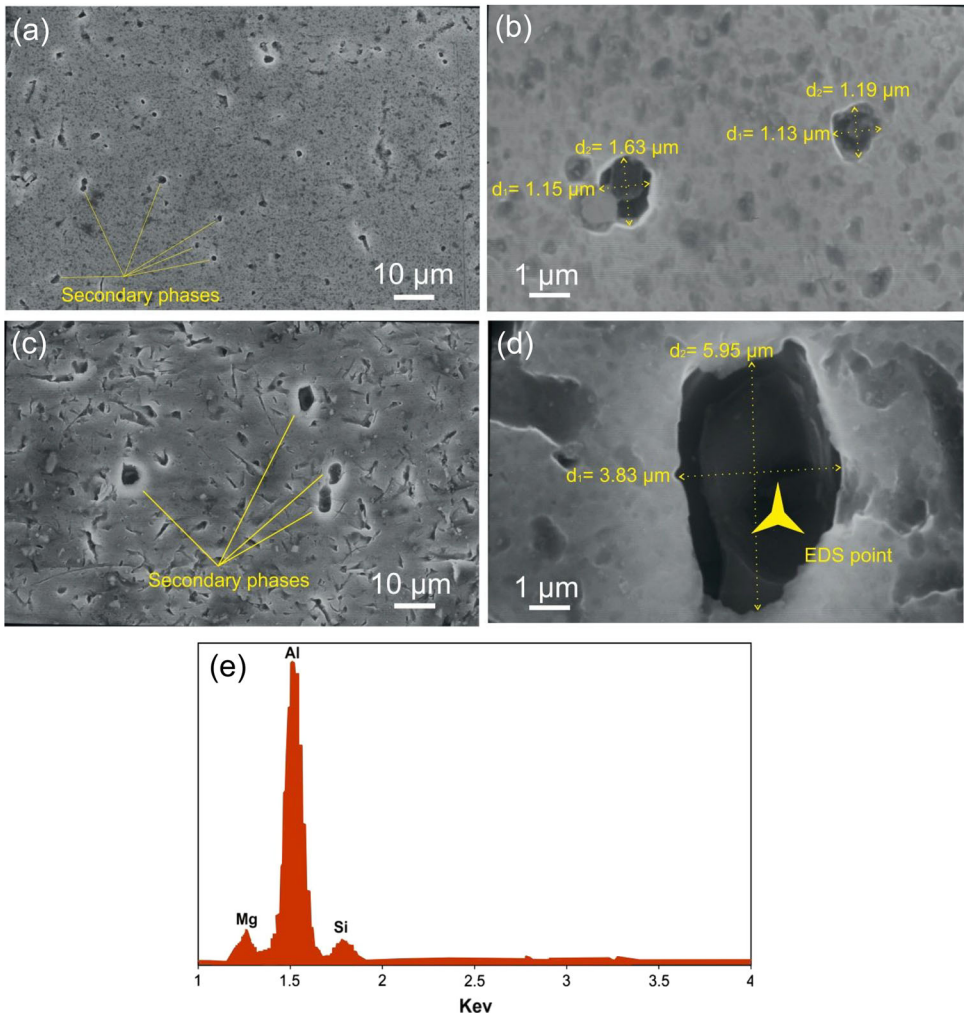

Fig. 4 SEM micrographs of (a, b) Al6061 BM and (c, d) five-pass FSPed Al6061 BM showing secondary phases coarsening and (e) corresponding EDS spectrum

Considering Fig. 4 which shows the SEM images taken from Al6061 base metal and SZ of five-pass FSPed Al6061 with the EDS spectrum of the secondary phases, it is obvious that the FSP has led to the coarsening of secondary phases. Also, regarding the XRD patterns of Al6061 base metal and five-pass FSPed composite which are presented in Fig. 5, applying FSP on the A6061 aluminum alloy has caused Mg_2Si peaks to be revealed. However, the intensity of this phase is very low that can be attributed to its low amount in the alloy's composition. Thus, it can be concluded from Fig. 4 and 5 that coarsening of the secondary phases is the reason for revealing the XRD peak of Mg_2Si. This phenomenon can affect the mechanical performance of the alloy.

It is worth noting that the grain refinement of aluminum is caused by dynamic recrystallization after FSP. During FSP, because of the high stacking fault energy of aluminum alloys, dislocations can easily glide/climb through dynamic recovery (DRV). It is important to note that the dynamic recrystallization can be continuous or discontinuous. In addition, to the initiation of the discontinuous dynamic recrystallization (DDRX) in any metal, there should be the following condition:

$$\frac{\rho_m^3}{\dot{\varepsilon}} > \frac{2\gamma_b}{KLMGb^5} \qquad \text{(Eq 1)}$$

where ρ_m is the density of mobile dislocations, $\dot{\varepsilon}$ is the strain rate, γ_b is the grain boundary energy, K is a constant fraction of the dislocation line energy that is stored in the newly formed grains, L is the mean slip distance of a dislocation in these grains, M is the boundary mobility, G is the shear modulus and b is the Burger's vector. The terms on the right-hand side of Eq 1 may be regarded as approximately constant at a particular temperature, and thus, the condition for the nucleation of DDRX is that a critical value of $\frac{\rho_m^3}{\dot{\varepsilon}}$ must be achieved. In materials such as aluminum and pure iron, recovery occurs readily and this parameter, strongly dependent on dislocation density, never reaches the critical value, and therefore, only dynamic recovery occurs. These conditions imply that aluminum and its alloys do not experience DDRX, because of their high rate of DRV. Therefore, it can be concluded that the continuous dynamic recrystallization (CDRX) is a possible recrystallization mechanism for aluminum alloys, during FSP (Ref 37-39).

Figure 6 illustrates the microstructures of the SZ of Al6061/SiO_2 surface composites fabricated by different pass numbers of FSP. It is clear that the size of SiO_2 particles in the sample after five passes of FSP is much smaller than the two-pass sample. In other words, the application of two-pass FSP seems

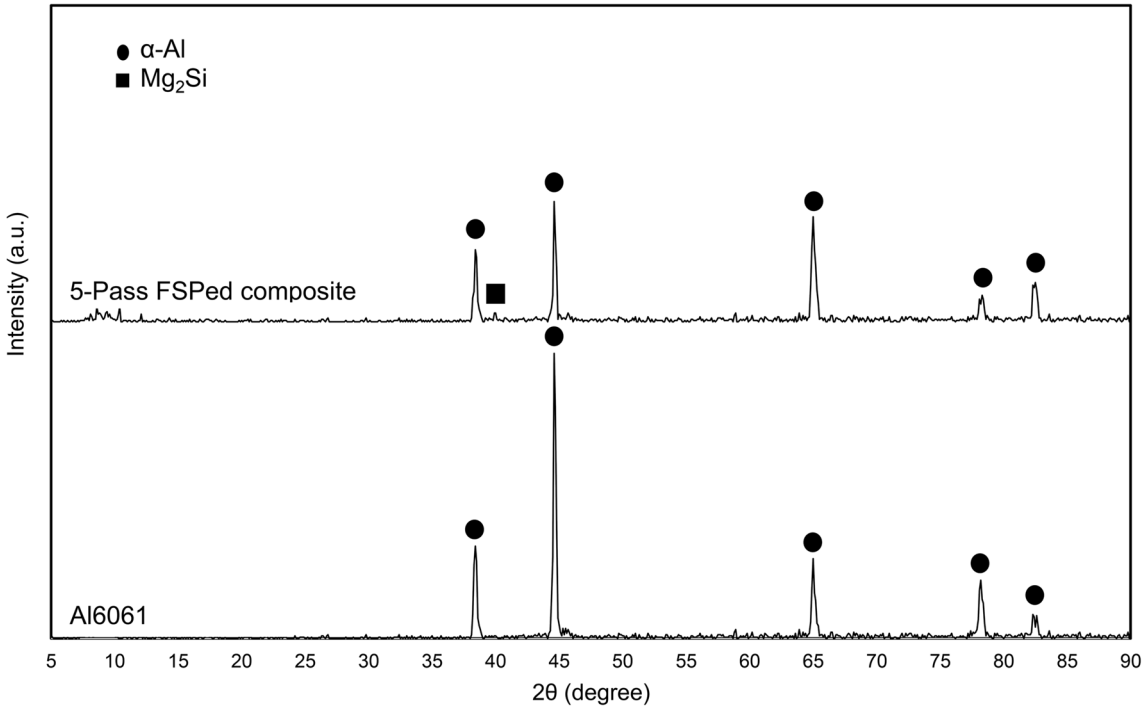

Fig. 5 The XRD patterns of Al6061 BM and five-pass FSPed composite

to be ineffective in case of the dispersion and distribution of SiO_2 particles. The agglomerated SiO_2 particles in two-pass FSPed sample seem to have a detrimental effect on the mechanical properties. In other words, by increasing the pass numbers, great refining of the particles size and also uniform distribution of SiO_2 particles is achievable.

Moreover, aluminum alloys contain secondary phases. The most important secondary phase in the Al6061 alloy is Mg_2Si precipitate (Ref 1). Increasing the temperature during FSP results in coarsening of the Mg_2Si precipitates. In addition, an increase in the number of FSP passes leads to higher heat rise and thus the precipitates become coarser (Ref 40).

3.2 Microhardness Measurements

The microhardness profiles of FSPed samples are illustrated in Fig. 7. Figure 7(a) shows the microhardness evolution of Al6061 base metal after two, three and five passes of FSP. As it can be seen, by increasing the pass number the microhardness of the stir zone decreased considerably. The diminution of microhardness for two and five passes is more than for three passes. In other words, the microhardness value of samples after two, three and five passes of FSP is about 11%, 26% and 33%, respectively, lower than that for the base metal. It should be noted that the Al6061 base metal was in T6 condition (see Fig. 3a) and had a microhardness value of about 100 HV. The high hardness value of the Al6061 can be attributed to the refined microstructure and homogenous distribution of the precipitates formed during heat treatment (Ref 1).

As mentioned before, FSP causes severe plastic deformation as well as a considerable heat generation (Ref 18, 40). These phenomena result in over aging and coarsening of the precipitates and consequently cause a reduction in the microhardness. In addition, as mentioned earlier, the grain refining phenomenon, because the recrystallization occurs during FSP, has an important effect on the microhardness evolution, according to well-known Hall–Petch relationship (Ref 41). In fact, the precipitates coarsening and grain refining are the competing phenomena where the former causes a decrease in the microhardness while the later causes an increase in the microhardness. It can be deduced that in the case of the three-pass FSPed sample the grain refinement had the dominant effect and prevents considerable microhardness depletion. However, it seems that for the five-pass FSPed sample, the coarsening was dominant and as a result of that considerable microhardness depletion was observed.

On the other hand, in the presence of SiO_2 particles, the microhardness evolution after different FSP passes was different. As shown in Fig. 7(b), the microhardness reduction after two and five passes was observed. However, the microhardness value of the three-pass FSPed Al6061/SiO_2 composites is about 10% higher than that of the base metal. In fact, it is well established that the incorporation of a second phase, in this case SiO_2 nanoparticles, in the aluminum matrix causes an increase in the strength values via several mechanisms such as pinning effect (Ref 42, 43), Orowan mechanism (Ref 12, 44), as well as the mismatch of the coefficients of thermal expansion (CTE) (Ref 14, 45). Accordingly, it can be deduced that for three-pass FSPed Al6061/SiO_2 composite, the strengthening mechanisms have a stronger role on mechanical properties and this sample had a maximum microhardness value. The decrease in microhardness was also reported by Hussain et al. after FSP of Al6061-SiO_2 surface composite (Ref 24). However, improving the microhardness value by adding particles or optimizing process parameters has been reported in some works (Ref 3, 26, 29, 31).

3.3 Wear Characteristics

Figure 8 illustrates the variations of weight losses of the samples with sliding distance after the wear tests. As can be seen, for all samples a gradually increasing trend in the weight

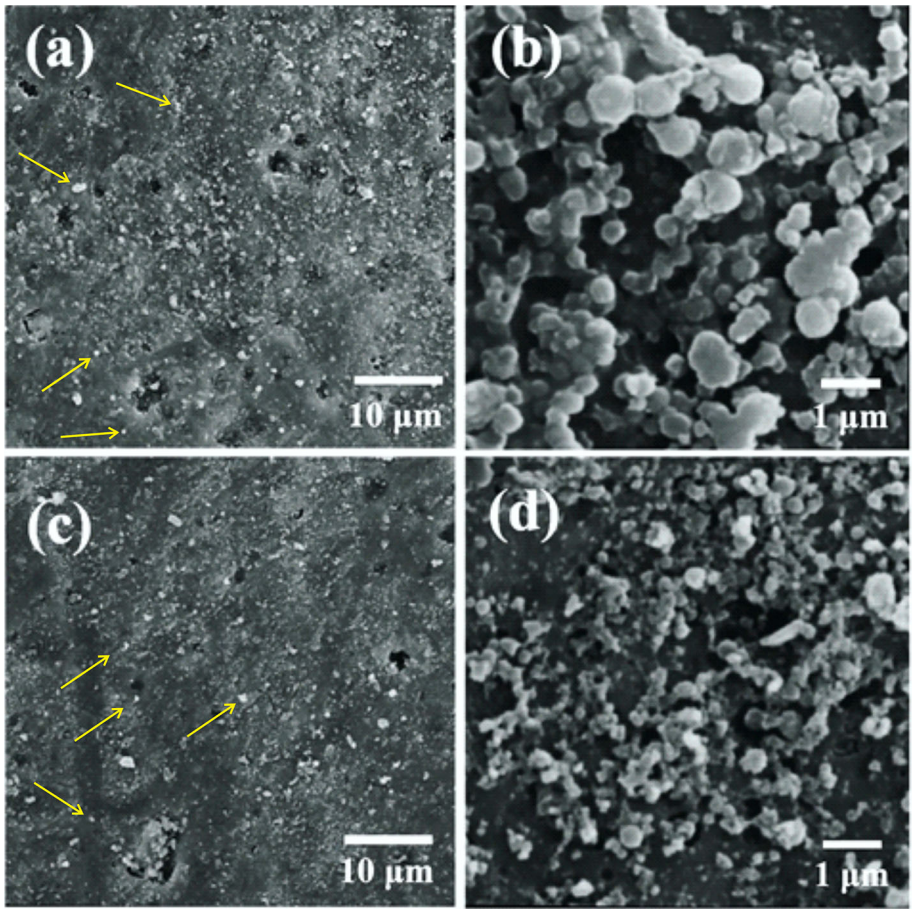

Fig. 6 SEM images of SZ of (a, b) two-pass and (c, d) five-pass FSPed Al6061/SiO_2 composites (arrows show SiO_2 particles)

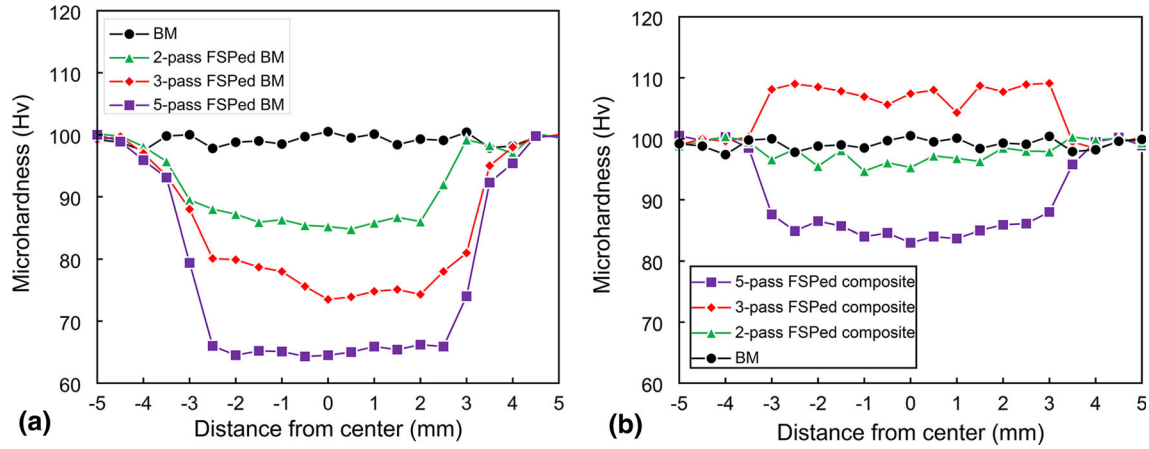

Fig. 7 The microhardness profile of the samples (a) without and (b) with SiO_2 particles

loss of samples as a function of sliding distance is observed. It is clear that for Al6061 and Al6061/SiO_2 composites, the highest weight loss of 70.8 mg and 31.3 mg is, respectively, obtained for two-pass FSPed Al6061 and Al6061/SiO_2 composites. In other words, the use of two passes of FSP has a negative effect on the wear properties of the samples. However, it seems that applying three- and five-pass FSP causes little decreasing in the weight loss of samples in comparison with the base metal. Also, it is clear that regarding the Al6061, the Al6061/SiO_2 composites have lower weight loss values. These results suggest that addition of SiO_2 particles exerts a powerful influence on wear behavior of the samples.

In addition, the dependence of friction coefficient and weight loss of the samples with the pass number of FSP is, respectively, given in Fig. 9(a) and (b). It can be seen that except for the two-pass FSPed samples, increasing the pass number causes a decrease in both friction coefficient and wear weight loss of the samples. Totally, it can be explained that increasing pass numbers of FSP, as well as the addition of SiO_2 particles, has a positive effect on the wear properties of the

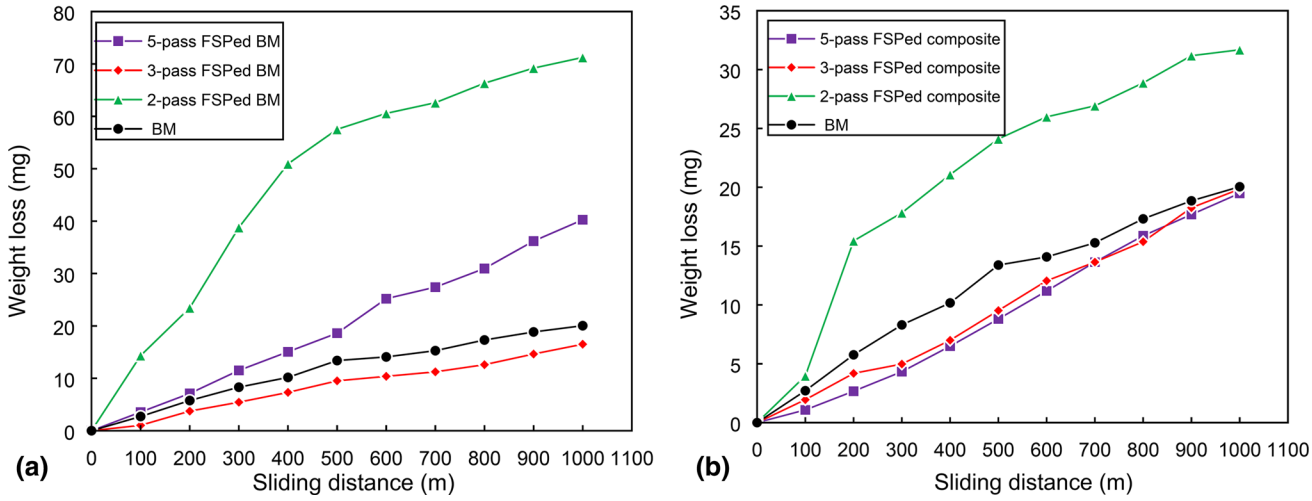

Fig. 8 The variation of the weight loss of samples (a) without and (b) with SiO_2 particles as a function of sliding distance

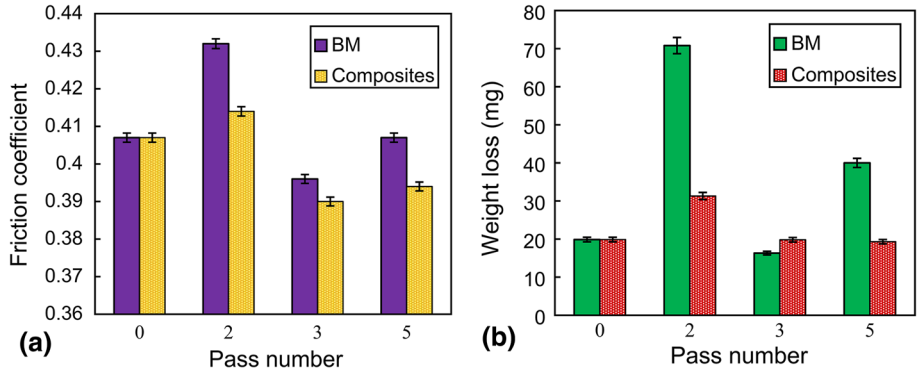

Fig. 9 The effect of pass number on the (a) friction coefficient and (b) wear weight loss of samples

samples. The weight loss and friction coefficient of the samples are presented in Table 1.

Considering the worn surface of BM and FSPed samples (Fig. 10), it is found that for two-pass FSPed samples, a severe plastic deformation has occurred. However, the worn surfaces of other samples are comparatively smooth. The features such as grooves, plowing and craters were observed on the worn surfaces. In addition, the EDS spectrum shown in Fig. 11 indicates no materials transfer from counterface to the substrate because all the peaks are originated from the Al6061 base metal. Therefore, it can be concluded that the wear mechanism is mainly abrasive.

The other remarkable point is related to the size of the wear debris. It is obvious that the wear debris of two-pass FSPed Al6061/SiO_2 composites is very large. On the other hand, increasing pass numbers results in a great reduction in debris size (Fig. 12). Therefore, it can be expressed that with pass numbers increasing, the wear mode changes from microcutting to the abrasive wear. This considerable improvement in wear properties of the samples with SiO_2 particles is mainly attributed to the following reasons:

(i) It is expected that the more materials possess microhardness, the higher they have wear resistance. Following equation correlate between hardness and volume loss of material, after wear testing (Ref 41, 46, 47):

Table 1 Results of wear testing including weight loss and friction coefficient of FSPed samples

Sample	Wear weight loss, mg	Friction coefficient
BM	19.86	0.407
Two-pass FSPed BM	70.8	0.432
Three-pass FSPed BM	16.3	0.396
Five-pass FSPed BM	40	0.407
Two-pass FSPed composite	31.3	0.414
Three-pass FSPed composite	19.8	0.390
Five-pass FSPed composite	19.3	0.394

$$Q = K\frac{W}{H} \quad \text{(Eq 2)}$$

where Q is the volume worn per unit sliding distance, W is the applied load, H is the hardness of the worn surface and K is the wear coefficient. As mentioned above, the maximum hardness value was obtained for the surface composite after three passes of FSP, and here, the minimum wear rate and friction coefficient were observed for this sample.

(ii) Another probable reason for the improvement in wear properties of the composites, containing SiO_2 nanoparti-

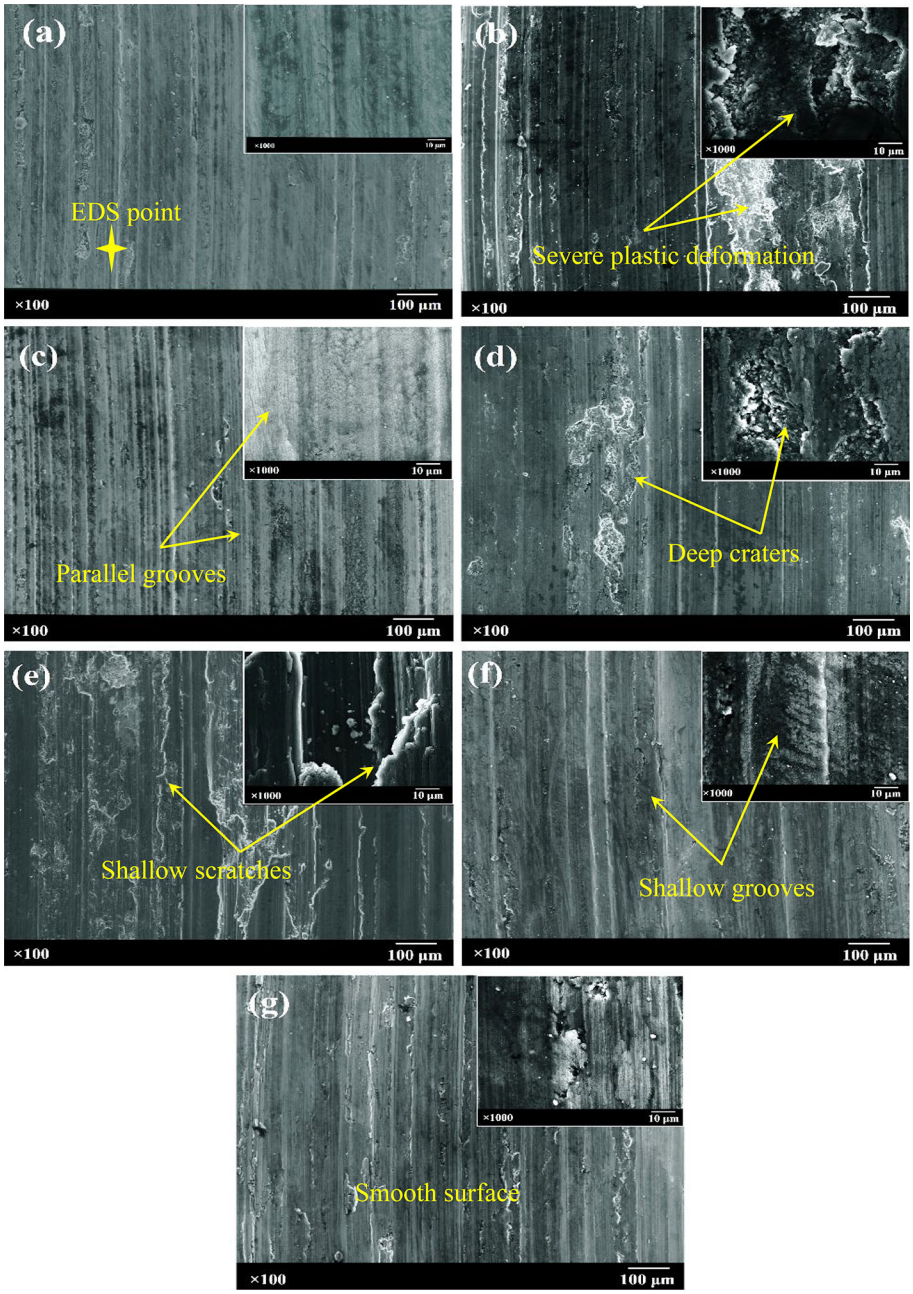

Fig. 10 SEM images of worn surface of the (a) BM, (b) two-pass, (c) three-pass and (d) five-pass FSPed BM, (e) two-pass, (f) three-pass and (g) five-pass FSPed Al6061/SiO_2 composites

cles, is the action of SiO_2 particles as a solid lubricant in this system. During sliding, there is found to be a partial pullout of the SiO_2 nanoparticles and consequently the tribofilm forms on the surface of the composites, leading to lowering the wear rate and friction coefficient values (Ref 3, 47).

(iii) As mentioned before, the dispersion condition of SiO_2 particles in two-pass FSPed samples was not suitable. In other words, it is the higher pass number that makes composites properties improve in terms of dispersion and distribution of SiO_2 particles. The SiO_2 nanoparticles properly would act as a barrier for the severe plastic deformation of samples under the wear loads (Ref 28).

(iv) It is of great importance that the difference between CTE of the aluminum and SiO_2 particles causes the development of the compressive residual stresses, hindering crack initiation and crack growth in composites (Ref 12, 48).

3.4 Corrosion Behavior

A few researchers have focused on the corrosion behavior of FSPed materials (Ref 49-53). Therefore, it is necessary to discuss the effects of FSP on the corrosion behavior of aluminum, especially Al6061. The potentiodynamic polarization curves of BM and FSPed samples in 3.5% NaCl solution are illustrated in Fig. 13. Moreover, the electrochemical

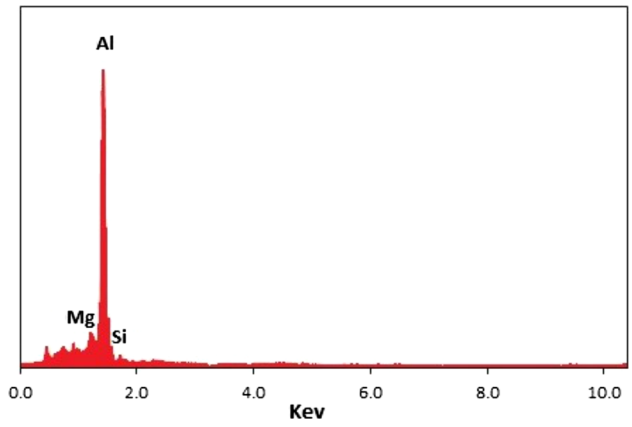

Fig. 11 EDS spectrum taken from the point marked in Fig. 10(a)

parameters of these samples are also given in Table 2. The corrosion potential and current density of Al6061 base metal are 0.6274 V and 63.65 μA/cm^2, respectively. The corrosion potential values of all FSPed samples (with or without SiO_2 addition) are less than that of the base metal, but their corrosion current density, except two-pass surface composite, is higher. This means that the corrosion resistance of FSPed samples is less than that of the base metal. In other words, the corrosion potential of the FSPed samples has been shifted to lower (active) values. So, it can be expressed that the application of FSP leads to the diminution of the corrosion resistance of Al6061. As mentioned earlier, some studies expressed that the FSP has a positive effect on the corrosion resistance (Ref 52), but some other studies reported that the FSP (or FSW) causes a reduction in corrosion resistance of Al6061 alloy (Ref 54-56).

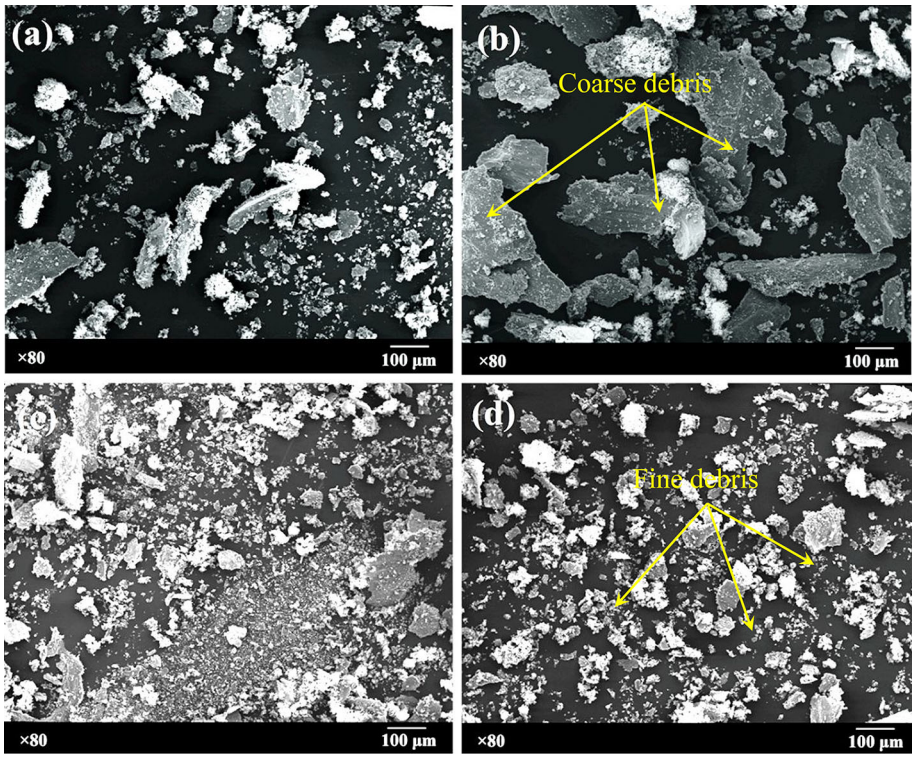

Fig. 12 The wear debris of (a) BM, (b) two-pass, (c) three-pass and (d) five-pass FSPed Al6061/SiO_2 composites

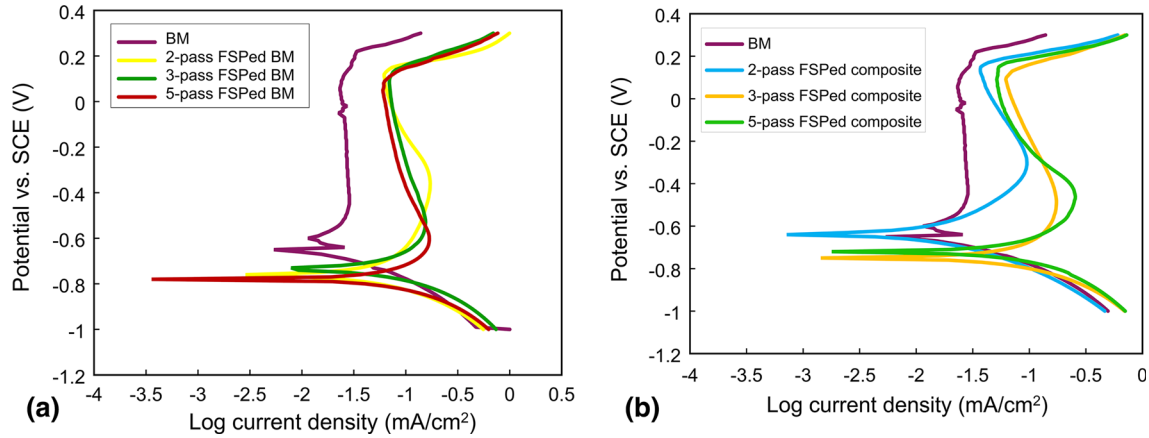

Fig. 13 Potentiodynamic polarization curves of samples (a) without and (b) with SiO_2 particles

Of course, there are several possible explanations for these findings:

(i) Undoubtedly existence of grains with small size follows a high density of grain boundary. Since the grain boundaries are more active than grains, the lower corrosion resistance of the FSPed samples in association with BM is a predictable circumstance (Ref 55). It is critical to note that the corrosion behavior of metals is remarkably sensitive to various factors comprehending the nature of metal, environment, etc.

(ii) As a well-known fact, SPD of FSP applies residual stress in parallel and perpendicular to the FSP direction. In addition, based on the Nernst equation, for samples with residual stresses the Gibbs free energy is higher; however, inversely electrical potential is lower than those for stressed-free samples (Ref 57). Accordingly, it seems reasonable to expect the lower corrosion resistance of FSPed samples than BM.

(iii) There are no doubts that Mg_2Si precipitates are known as the major intermetallic particles of the Al6061 (Ref 1). Furthermore, the activity of the Mg_2Si is higher than that of aluminum. Hence, the heat input of FSP led to the coarsening of the Mg_2Si and precipitated particles in the grain boundaries of aluminum can be dissolved, immersing in 3.5% NaCl solution. Then, these coarse precipitates are susceptible to intergranular or inter-subgranular corrosion (Ref 54). For example, the SEM images from the SZ zone of the two-pass FSPed Al6061/SiO_2 composite after polarization tests are illustrated in Fig. 14. As shown, a large number of corrosion pits with the size of 20-50 μm are visible for FSP processed samples (Fig. 14b). The appearance of microscale pits can be attributed to the presence of Mg_2Si precipitates in Al6061. Therefore, it can be expected that the higher heat input in FSP has caused coarsening of the Mg_2Si precipitates and consequently increasing the pitting corrosion of the samples. However, in the literature, there could be found diverse examples for merits of grain refining related to the corrosion resistance of aluminum (Ref 49, 50).

Table 2 The corrosion parameters of BM and FSPed samples

Material	I_{corr}, μA/cm^2	E_{corr}, V	R_P, ohm
BM	− 0.6574	63.65	886.1
Two-pass FSPed BM	− 0.7539	199.50	282.7
Three-pass FSPed BM	− 0.7272	260.23	217.3
Five-pass FSPed BM	− 0.7735	301.31	187.4
Two-pass FSPed composite	− 0.6326	56.99	989.7
Three-pass FSPed composite	− 0.7260	255.10	221.1
Five-pass FSPed composite	− 0.7157	297.61	189.6

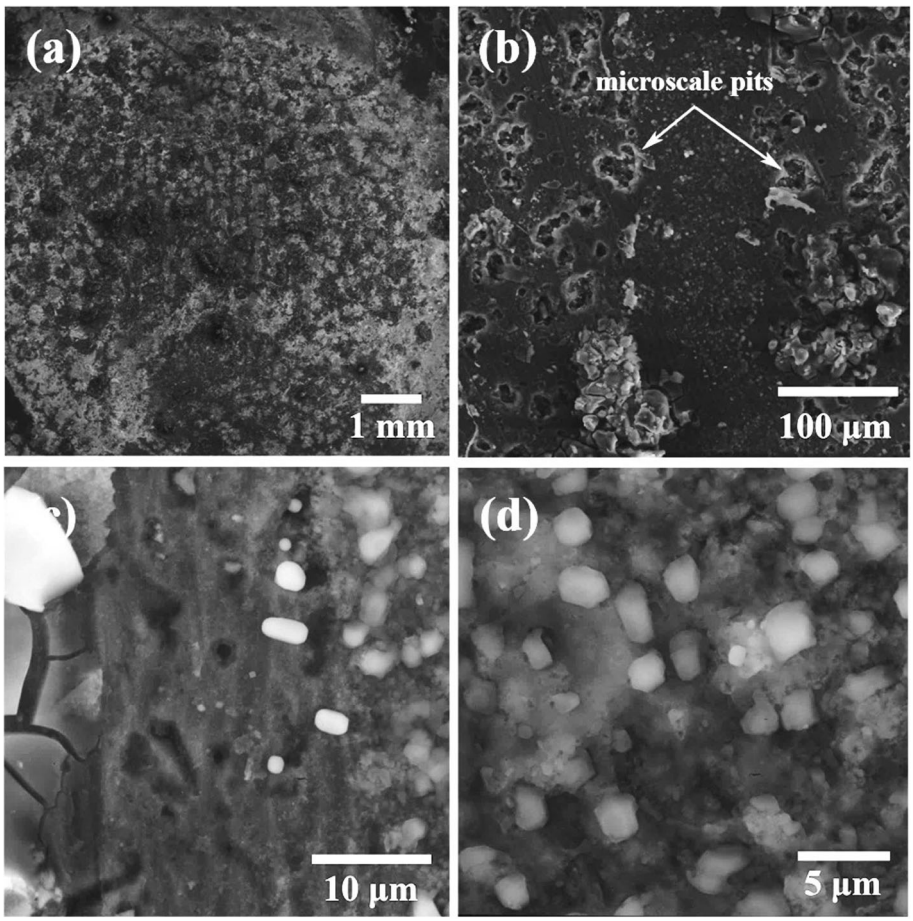

Fig. 14 The SZ of the two-pass FSPed Al6061/SiO_2 composite after corrosion testing (a, b) in smaller magnifications and (c, d) in higher magnifications

4. Conclusions

In this study, the Al6061 aluminum alloy was subjected to FSP in different passes. Also the SiO_2 nanoparticles were incorporated in the alloy during FSP to make the surface composite. The microhardness, wear and corrosion behavior of specimens were investigated, and the following conclusions were drawn:

(1) Microstructural investigations showed that FSP caused grain refinement, and by adding SiO_2 particles, this refinement intensified. By increasing the passes number, the dispersion of SiO_2 particles became more homogenous.
(2) As a consequence of the reduction in dislocations density and coarsening of Mg_2Si phases, the microhardness profile of FSPed samples showed general softening compared with the base metal. Only after three passes of FSP and in the presence of SiO_2 particles, the microhardness of the stir zone increased about 10%.
(3) Tribological investigation showed that after three passes of FSP, with or without SiO_2 particles, the wear resistance enhanced because of the higher hardness, acceptable grain refinement and homogenous distribution of the SiO_2 particles. Other specimens had lower wear resistance than the base alloy.
(4) The corrosion resistance of the FSPed samples, with or without SiO_2 particles, was destroyed in comparison with Al6061 base alloy due to the grain refinement and coarsening of Mg_2Si.

References

1. I.J. Polmear, D.S. John, J.F. Nie, and M. Qian, *Light alloys: metallurgy of the light metals*, 5th ed., Elsevier Ltd, Amsterdam, 2017
2. F.C. Campbell, Manufacturing Technology for Aerospace Structural Materials (2006). https://doi.org/10.1016/b978-185617495-4/50002-0
3. D. Aruri, K. Adepu, K. Adepu, and K. Bazavada, Wear and Mechanical Properties of 6061-T6 Aluminum Alloy Surface Hybrid Composites [(SiC + Gr) and (SiC + Al_2O_3)] Fabricated by Friction Stir Processing, *J. Mater. Res. Technol.*, 2013, **2**, p 362–369. https://doi.org/10.1016/j.jmrt.2013.10.004
4. D.B. Miracle, Metal Matrix Composites—from Science to Technological Significance, *Compos. Sci. Technol.*, 2005, **65**, p 2526–2540. https://doi.org/10.1016/j.compscitech.2005.05.027
5. H. Chen, W. Wang, H. Nie, J. Zhou, Y. Li, and P. Zhang, Microstructure and Mechanical Properties of B4C/6061Al Laminar Composites Fabricated by Power Metallurgy, *Vacuum*, 2017, **143**, p 363–370. https://doi.org/10.1016/j.vacuum.2017.06.009
6. S. Lü, P. Xiao, D. Yuan, K. Hu, and S. Wu, Preparation of Al Matrix Nanocomposites by Diluting the Composite Granules Containing Nano-SiCp Under Ultrasonic Vibration, *J. Mater. Sci. Technol.*, 2018, **34**, p 1609–1617. https://doi.org/10.1016/j.jmst.2018.01.003
7. B.C. Kandpal, J. Kumar, and H. Singh, Manufacturing and Technological Challenges in Stir Casting of Metal Matrix Composites—A Review, *Mater. Today Proc.*, 2018, **5**, p 5–10. https://doi.org/10.1016/j.matpr.2017.11.046
8. S.M.Y. Kaku, A.K. Khanra, and M.J. Davidson, Effect of Deformation on Properties of Al/Al-alloy ZrB2 Powder Metallurgy Composite, *J. Alloys Compd.*, 2018, **747**, p 666–675. https://doi.org/10.1016/j.jallcom.2018.03.088
9. A.N. Attia, Surface Metal Matrix Composites, *Mater. Des.*, 2001, **22**, p 451–457. https://doi.org/10.1016/S0261-3069(00)00081-9
10. A. Kurt, I. Uygur, and E. Cete, Surface Modification of Aluminium by Friction Stir Processing, *J. Mater. Process. Technol.*, 2011, **211**, p 313–317. https://doi.org/10.1016/j.jmatprotec.2010.09.020
11. S. Dejiu, C. Jingrui, L. Guolong, H. Donglei, W. Lailei, M. Haojie, X. Yonghong, C. He, and Y. Yaqian, Effect of Ultrasonic on Microstructure and Growth Characteristics of Micro-Arc Oxidation Ceramic Coatings on 6061 Aluminum Alloy, *Vacuum*, 2014, **99**, p 143–148. https://doi.org/10.1016/j.vacuum.2013.05.022
12. H.S. Arora, H. Singh, and B.K. Dhindaw, Composite Fabrication Using Friction Stir Processing—A Review, *Int. J. Adv. Manuf. Technol.*, 2012, **61**, p 1043–1055. https://doi.org/10.1007/s00170-011-3758-8
13. M.S. Węglowski, Friction Stir Processing—State of the Art, *Arch. Civ. Mech. Eng.*, 2018, **18**, p 114–129. https://doi.org/10.1016/j.acme.2017.06.002
14. S. Rathee, S. Maheshwari, and A.N. Siddiquee, Issues and Strategies in Composite Fabrication via Friction Stir Processing: A Review, *Mater. Manuf. Process.*, 2018, **33**, p 239–261. https://doi.org/10.1080/10426914.2017.1303162
15. S. Rathee, S. Maheshwari, A.N. Siddiquee, and M. Srivastava, Distribution of Reinforcement Particles in Surface Composite Fabrication via Friction Stir Processing: Suitable Strategy, *Mater. Manuf. Process.*, 2018, **33**, p 262–269. https://doi.org/10.1080/10426914.2017.1303147
16. Z. Ding, C. Zhang, L. Xie, L.-C. Zhang, L. Wang, and W. Lu, Effects of Friction Stir Processing on the Phase Transformation and Microstructure of TiO_2-Compounded Ti–6Al-4V Alloy, *Metall. Mater. Trans. A*, 2016, https://doi.org/10.1007/s11661-016-3809-8
17. P. Liu, Y. Li, G. Zhang, and K. Feng, Relation Between Thermal Effect and Phase Transformation of Aluminium Matrix Surface Composite Adding Al-Based Amorphous Fabricated by FSP, *Vacuum*, 2016, **131**, p 65–68. https://doi.org/10.1016/j.vacuum.2016.06.002
18. Z.Y. Ma, Friction Stir Processing Technology: A Review, *Metall. Mater. Trans. A*, 2008, **39**, p 642–658. https://doi.org/10.1007/s11661-007-9459-0
19. S. Kumar, S.K. Reddy, and S.V. Joshi, Microstructure and Performance of Cold Sprayed Al–SiC Composite Coatings with High Fraction of Particulates, *Surf. Coat. Technol.*, 2017, **318**, p 62–71. https://doi.org/10.1016/j.surfcoat.2016.11.047
20. A. Sharma, V.M. Sharma, S. Mewar, S.K. Pal, and J. Paul, Friction Stir Processing of Al6061-SiC-Graphite Hybrid Surface Composites, *Mater. Manuf. Process.*, 2018, **33**, p 795–804. https://doi.org/10.1080/10426914.2017.1401726
21. M. Salehi, M. Saadatmand, and J.A. Mohandesi, Optimization of Process Parameters for Producing AA6061/SiC Nanocomposites by Friction Stir Processing, *Trans. Nonferrous Met. Soc. China*, 2012, **22**, p 1055–1063. https://doi.org/10.1016/S1003-6326(11)61283-1
22. D.H. Choi, Y. Il Kim, D.U. Kim, and S.B. Jung, Effect of SiC Particles on Microstructure and Mechanical Property of Friction Stir Processed AA6061-T4, *Trans. Nonferrous Met. Soc. China (Engl. Ed.)*, 2012, **22**, p s614–s618. https://doi.org/10.1016/s1003-6326(12)61773-7
23. S. Rathee, S. Maheshwari, A.N. Siddiquee, M. Srivastava, and S.K. Sharma, Process Parameters Optimization for Enhanced Microhardness of AA 6061/SiC Surface Composites Fabricated via Friction Stir Processing (FSP), *Mater. Today Proc.*, 2016, **3**, p 4151–4156. https://doi.org/10.1016/j.matpr.2016.11.089
24. H. Zuhailawati, M.N. Halmy, I.P. Almanar, and B.K. Dhindaw, Friction Stir Processed of 6061-T6 Aluminum Alloy Reinforced with Silica from Rice Husk Ash, *Adv. Mater. Res.*, 2014, **1024**, p 227–230. https://doi.org/10.4028/www.scientific.net/AMR.1024.227
25. A. Devaraju, A. Kumar, and B. Kotiveerachari, Influence of Addition of Grp/Al_2O_3p with SiCp on Wear Properties of Aluminum alloy 6061-T6 Hybrid Composites via Friction Stir Processing, *Trans. Nonferrous Met. Soc. China (Engl. Ed.)*, 2013, https://doi.org/10.1016/s1003-6326(13)62593-5
26. K. Zhao, Z.Y. Liu, B.L. Xiao, D.R. Ni, and Z.Y. Ma, Origin of Insignificant Strengthening Effect of CNTs in T6-Treated CNT/6061Al Composites, *Acta Metall. Sin. (Engl. Lett.)*, 2018, **31**, p 134–142. https://doi.org/10.1007/s40195-017-0626-z
27. Z.Y. Liu, B.L. Xiao, W.G. Wang, and Z.Y. Ma, Tensile Strength and Electrical Conductivity of Carbon Nanotube Reinforced Aluminum Matrix Composites Fabricated by Powder Metallurgy Combined with Friction Stir Processing, *J. Mater. Sci. Technol.*, 2014, **30**, p 649–655. https://doi.org/10.1016/j.jmst.2014.04.016

28. A. Devaraju, A. Kumar, and B. Kotiveerachari, Influence of Rotational Speed and Reinforcements on Wear and Mechanical Properties of Aluminum Hybrid Composites via Friction Stir processing, *Mater. Des.*, 2013, **45**, p 576–585. https://doi.org/10.1016/j.matdes.2012.09.036
29. D.R. Ni, J.J. Wang, Z.N. Zhou, and Z.Y. Ma, Fabrication and Mechanical Properties of Bulk NiTip/Al Composites Prepared by Friction Stir Processing, *J. Alloys Compd.*, 2014, **586**, p 368–374. https://doi.org/10.1016/j.jallcom.2013.10.013
30. V. Kishan, A. Devaraju, and K.P. Lakshmi, Tribological Properties of Bano TiB_2 Particle Reinforced 6061-T6 Aluminum Alloy Surface Composites via Friction Stir Processing, *Mater. Today Proc.*, 2018, **5**, p 1615–1619. https://doi.org/10.1016/j.matpr.2017.11.254
31. V. Kishan, A. Devaraju, and K.P. Lakshmi, Influence of Volume Percentage of NanoTiB_2 Particles on Tribological & Mechanical Behaviour of 6061-T6 Al Alloy Nano-surface Composite Layer Prepared via Friction Stir Process, *Def. Technol.*, 2017, **13**, p 16–21. https://doi.org/10.1016/j.dt.2016.11.002
32. D.C. Hofmann and K.S. Vecchio, Submerged Friction Stir Processing (SFSP): An Improved Method for Creating Ultra-Fine-Grained Bulk Materials, *Mater. Sci. Eng. A*, 2005, **402**, p 234–241. https://doi.org/10.1016/j.msea.2005.04.032
33. A. Ebnonnasir, F. Karimzadeh, and M.H. Enayati, Novel Artificial Neural Network Model for Evaluating Hardness of Stir Zone of Submerge Friction Stir Processed Al 6061-T6 Plate, *Mater. Sci. Technol.*, 2011, **27**, p 990–995. https://doi.org/10.1179/174328409X425290
34. M.M. Jalilvand, Y. Mazaheri, A. Heidarpour, and M. Roknian, Development of A356/Al_2O_3 + SiO_2 Surface Hybrid Nanocomposite by Friction Stir Processing, *Surf. Coat. Technol.*, 2019, **360**, p 121–132. https://doi.org/10.1016/j.surfcoat.2018.12.126
35. ASTM E384–17, *Standard test method for microindentation hardness of materials*, ASTM International, West Conshohocken, 2017
36. ASTM G99–17, *Standard test method for wear testing with a pin-on-disk apparatus*, ASTM International, West Conshohocken, 2017
37. T.R. McNelley, S. Swaminathan, and J.Q. Su, Recrystallization Mechanisms During Friction Stir Welding/Processing of Aluminum Alloys, *Scr. Mater.*, 2008, **58**, p 349–354. https://doi.org/10.1016/j.scriptamat.2007.09.064
38. F. Humphreys and M. Matherly, *Recrystallization and related annealing phenomena*, Elsevier Sci. Ltd Publ., New York, 1995, p 173–178
39. F.J. Humphreys, P.B. Prangnell, and R. Priestner, Fine-Grained Alloys by Thermomechanical Processing, *Curr. Opin. Solid State Mater. Sci.*, 2001, **5**, p 15–21. https://doi.org/10.1016/S1359-0286(00)00020-6
40. R.S. Mishra and Z.Y. Ma, Friction Stir Welding and Processing, *Mater. Sci. Eng. R Rep.*, 2005, **50**, p 1–78. https://doi.org/10.1016/j.mser.2005.07.001
41. Y. Mazaheri, F. Karimzadeh, and M.H. Enayati, Tribological Behavior of A356/Al2O3 Surface Nanocomposite Prepared by Friction Stir Processing, *Metall. Mater. Trans. A*, 2014, **45**, p 2250–2259. https://doi.org/10.1007/s11661-013-2140-x
42. J.F. Guo, J. Liu, C.N. Sun, S. Maleksaeedi, G. Bi, M.J. Tan, and J. Wei, Effects of Nano-Al_2O_3 Particle Addition on Grain Structure Evolution and Mechanical Behaviour of Friction-Stir-Processed Al, *Mater. Sci. Eng. A*, 2014, **602**, p 143–149. https://doi.org/10.1016/j.msea.2014.02.022
43. S. Ahmadifard, S. Kazemi, and A. Heidarpour, Production and Characterization of A5083-Al_2O_3–TiO_2 Hybrid Surface Nanocomposite by Friction Stir Processing, *Proc. Inst. Mech. Eng. Part L J. Mater. Des. Appl.*, 2018, **232**, p 287–293. https://doi.org/10.1177/1464420715623977
44. R. Yang, Z. Zhang, Y. Zhao, G. Chen, Y. Guo, M. Liu, and J. Zhang, Materials Characterization Effect of Multi-Pass Friction Stir Processing on Microstructure and Mechanical Properties of Al_3Ti/A356 Composites, *Mater. Charact.*, 2015, **106**, p 62–69. https://doi.org/10.1016/j.matchar.2015.05.019
45. K.-M. Lee, D.-K. Oh, W.-S. Choi, T. Weissgärber, and B. Kieback, Thermomechanical Properties of AlN–Cu Composite Materials Prepared by Solid State Processing, *J. Alloys Compd.*, 2007, **434–435**, p 375–377. https://doi.org/10.1016/j.jallcom.2006.08.176
46. C.Y.H. Lim, S.C. Lim, and M. Gupta, Wear Behaviour of SiCp-Reinforced Magnesium Matrix Composites, *Wear*, 2003, **255**, p 629–637. https://doi.org/10.1016/S0043-1648(03)00121-2
47. M. Akbari, M.H. Shojaeefard, P. Asadi, and A. Khalkhali, Wear and Mechanical Properties of Surface Hybrid Metal Matrix Composites on Al–Si Aluminum Alloys Fabricated by Friction Stir Processing, *Proc. Inst. Mech. Eng. Part L J. Mater. Des. Appl.*, 2017, **233**, p 790–799. https://doi.org/10.1177/1464420717702413
48. C.J. Hsu, C.P.Y. Chang, P.W. Kao, N.J. Ho, and C.P.Y. Chang, Al-Al3Ti Nanocomposites Produced in situ by Friction Stir Processing, *Acta Mater.*, 2006, **54**, p 5241–5249. https://doi.org/10.1016/j.actamat.2006.06.054
49. A.G. Rao, V.A. Katkar, G. Gunasekaran, V.P. Deshmukh, N. Prabhu, and B.P. Kashyap, Effect of Multipass Friction Stir Processing on Corrosion Resistance of Hypereutectic Al-30Si Alloy, *Corros. Sci.*, 2014, **83**, p 198–208. https://doi.org/10.1016/j.corsci.2014.02.013
50. K. Surekha, B.S. Murty, and K.P. Rao, Microstructural Characterization and Corrosion Behavior of Multipass Friction Stir Processed AA2219 Aluminium Alloy, *Surf. Coat. Technol.*, 2008, **202**, p 4057–4068. https://doi.org/10.1016/j.surfcoat.2008.02.001
51. K. Surekha, B.S. Murty, and K. Prasad Rao, Comparison of Corrosion Behaviour of Friction Stir Processed and Laser Melted AA 2219 Aluminium Alloy, *Mater. Des.*, 2011, **32**, p 4502–4508. https://doi.org/10.1016/j.matdes.2011.03.033
52. R.A. Behnagh, M.K. Besharati Givi, and M. Akbari, Mechanical Properties, Corrosion Resistance, and Microstructural Changes During Friction Stir Processing of 5083 Aluminum Rolled Plates, *Mater. Manuf. Process.*, 2012, **27**, p 636–640. https://doi.org/10.1080/10426914.2011.593243
53. M. Amra, K. Ranjbar, and R. Dehmolaei, Mechanical Properties and Corrosion Behavior of CeO_2 and SiC Incorporated Al5083 Alloy Surface Composites, *J. Mater. Eng. Perform.*, 2015, **24**, p 3169–3179. https://doi.org/10.1007/s11665-015-1596-9
54. F. Gharavi, K.A. Matori, R. Yunus, N.K. Othman, and F. Fadaeifard, Corrosion Behavior of Al6061 Alloy Weldment Produced by Friction Stir Welding Process, *J. Mater. Res. Technol.*, 2015, **4**, p 314–322. https://doi.org/10.1016/j.jmrt.2015.01.007
55. J.F. Flores, A. Neville, N. Kapur, and A. Gnanavelu, Corrosion and Erosion-Corrosion Processes of Metal-Matrix Composites in Slurry Conditions, *J. Mater. Eng. Perform.*, 2012, **21**, p 395–405. https://doi.org/10.1007/s11665-011-9926-z
56. V. Fahimpour, S.K. Sadrnezhaad, and F. Karimzadeh, Corrosion Behavior of Aluminum 6061 Alloy Joined by Friction Stir Welding and Gas Tungsten Arc Welding Methods, *Mater. Des.*, 2012, **39**, p 329–333. https://doi.org/10.1016/j.matdes.2012.02.043
57. D.R. Ni, B.L. Xiao, Z.Y. Ma, Y.X. Qiao, and Y.G. Zheng, Corrosion Properties of Friction-Stir Processed Cast NiAl Bronze, *Corros. Sci.*, 2010, **52**, p 1610–1617. https://doi.org/10.1016/j.corsci.2010.02.026